Two-dimensional Determination of the Decision Boundary for a Radar Detection Method in the Moment Space

Camilo Guillén[1]*, Nelson Chávez[1]

Guillén C　[iD]　http://orcid.org/0000-0001-9538-3099
Chávez N　[iD]　https://orcid.org/0000-0001-6580-9095

ABSTRACT: The radar detection with decision making in the moments space (DRACEC method) is based on a statistical analysis to determine the boundary between the background (absent target) and the anomaly (present target) classes. In this article, the boundary is taken as an ellipse and is calculated for two dimensions, emphasizing its geometric interpretation. The procedures to establish the shape, location, and size of the ellipse are highlighted, guaranteeing the probability of false alarm by applying the Neyman-Pearson criterion. The proposal establishes a methodology for calculation of the boundary when it is required to use the moments directly as a sufficient decision statistic.

KEYWORDS: Radar, DRACEC method, Moment space, Decision boundary.

INTRODUCTION

The fundamental detection problem lies in the computation of the boundary between the two classes according to some optimization criterion. One of the most used criteria is the Bayes' rule (Kay 1998; Webb 2002; Bishop 2006), which employs the likelihood ratio to minimize the average cost of possible decisions. In radars, the decisions are to establish whether the received signal corresponds to noise (absent target) or if it is a useful signal in addition to noise (present target). With this purpose, the Neyman-Pearson criterion, derived from the Bayes' rule, is used; it ignores the a priori knowledge of costs and it is based on fixing the false alarm probability (P_{FA}) while maximizing the detection probability (P_D) (DiFranco and Rubin 2004; Richards *et al.* 2010).

The DRACEC method (DRACEC is an Spanish acronym for Radar target Detection by Analysis and Statistical Classification of the Cellular Emission) (Chávez 2002; Chávez and Guillén 2018) applies the aforementioned criteria with a notable difference with respect to conventional techniques: instead of using echo signal parameters for detection (amplitude, phase, frequency, etc.), it uses a function of some of their moments (mean, second order moment, correlation, etc.). Hence, DRACEC is regarded as a detection method in the moment space. The moment's function is referred to as sufficient decision statistics (SDS), which is obtained from the likelihood ratio, and therefore transforms the input random variables seeking to optimally differentiate their possible states. A common SDS for the classic radar techniques is the correlation of the received signal with a proper replica (DiFranco and Rubin 2004; Richards *et al.* 2010).

1.Universidad Tecnológica de la Habana José Antonio Echeverría – Facultad de Telecomunicaciones y Electrónica – Departamento de Telecomunicaciones y Telemática – La Habana – Cuba.

Correspondence author: camilo.gs@tele.cujae.edu.cu

To guarantee the P_{FA}, DRACEC requires to estimate the detection threshold using the SDS Probability Density Function (PDF) (Chávez and Guillén 2018). Although this threshold has a direct representation in the SDS domain, it is useful to analyze its equivalent in the moments space: the decision boundary (Chávez and González 2008). It is possible to establish different ways to calculate the boundary knowing the relationship between both domains, which could be convenient depending on the application scenario. This article proposes a geometric approach that establishes a link between the boundary in the moment space and the corresponding SDS threshold. Using the relationship between both domains, a procedure is proposed to determine the shape, size, and location of the boundary through the Neyman-Pearson criterion. The analysis is done for the case when the boundary is an ellipse and only two moments are considered in order to visualize the results in a simple way.

DETERMINATION OF THE DECISION BOUNDARY

The DRACEC point of view is based on the fact that since the noise is always present, the signal scattered by the target is the one that disturbs the "normality" of the received signal. The searching region is divided into resolution cells, each of which, due to the phenomenon of secondary emission, originates an electromagnetic field that can be considered as the cell response. By means of a statistical analysis of this response, a classification vector (pattern) is obtained whose components (features) are some of its statistical moments, which allows to classify the cell into the *background* class or the *anomaly* class.

For this cellular emission classification, it is necessary to determine the decision threshold applying the Neyman-Pearson criterion (Kay 1998; DiFranco and Rubin 2004; Richards *et al.* 2010), which implies to obtain the SDS in relation to the two possible hypotheses: *background* or *anomaly*. When the size of the parameter sample is large enough, its moments will form a new random variable that is Gaussian distributed (Korn and Korn 1968; Koroliuk 1981). Consequently, considering the case of two statistically independent moments m_1 and m_2, the likelihood ratio will be expressed by:

$$\Lambda(m_1, m_2) = \frac{p_A(m_1, m_2)}{p_B(m_1, m_2)} = \frac{p_A(m_1) p_A(m_2)}{p_B(m_1) p_B(m_2)} = \frac{\frac{1}{\sqrt{2\pi}\,\sigma_{A,1}^P} \exp\left[-\frac{\left(m_1 - m_{A,1}^P\right)^2}{2\left(\sigma_{A,1}^P\right)^2}\right] \frac{1}{\sqrt{2\pi}\,\sigma_{A,2}^P} \exp\left[-\frac{\left(m_2 - m_{A,2}^P\right)^2}{2\left(\sigma_{A,2}^P\right)^2}\right]}{\frac{1}{\sqrt{2\pi}\,\sigma_{B,1}^P} \exp\left[-\frac{\left(m_1 - m_{B,1}^P\right)^2}{2\left(\sigma_{B,1}^P\right)^2}\right] \frac{1}{\sqrt{2\pi}\,\sigma_{B,2}^P} \exp\left[-\frac{\left(m_2 - m_{B,2}^P\right)^2}{2\left(\sigma_{B,2}^P\right)^2}\right]} \tag{1}$$

where: $p_A(m_1), p_A(m_2), p_B(m_1)$, and $p_B(m_2)$ are the PDF for the moments, subscripts A and B identify the *anomaly* and *background* classes, respectively, and P in the superscripts indicates the population means ($m_{A,1}^P$, $m_{A,2}^P$, $m_{B,1}^P$, $m_{B,2}^P$) and variances ($\sigma_{A,1}^P$, $\sigma_{A,2}^P$, $\sigma_{B,1}^P$, $\sigma_{B,2}^P$) for the proper moment and class.

Starting from Eq. 1 and after several algebraic manipulations, the likelihood ratio can be expressed in the form:

$$\Lambda(m_1, m_2) = \frac{\sigma_{B,1}^P \sigma_{B,2}^P}{\sigma_{A,1}^P \sigma_{A,2}^P} e^Z \tag{2}$$

where:

$$Z = a_1\, m_1^2 + b_1\, m_1 + c_1 + a_2\, m_2^2 + b_2\, m_2 + c_2 \tag{3}$$

and

$$a_s = \frac{\left(\sigma_{A,s}^P\right)^2 - \left(\sigma_{B,s}^P\right)^2}{2\left(\sigma_{A,s}^P\right)^2 \left(\sigma_{B,s}^P\right)^2} \qquad s = 1, 2 \tag{4}$$

$$b_s = \frac{\left(\sigma_{B,s}^P\right)^2 m_{A,s}^P - \left(\sigma_{A,s}^P\right)^2 m_{B,s}^P}{\left(\sigma_{A,s}^P\right)^2 \left(\sigma_{B,s}^P\right)^2} \qquad s = 1, 2 \tag{5}$$

$$c_s = \left[\frac{\left(m_{B,s}^P\right)^2}{2\left(\sigma_{B,s}^P\right)^2} - \frac{\left(m_{A,s}^P\right)^2}{2\left(\sigma_{A,s}^P\right)^2}\right] \qquad s = 1, 2 \tag{6}$$

As it is observed in Eq. 2, the likelihood ratio is monotonically increasing with Z, so the latter can be used to calculate the decision threshold directly, since $Z > Z_0$ implies that $\Lambda > \Lambda_0$. For this reason, Z is established as SDS. Eq. 3 shows the quadratic dependence of the moments presented by Z and it should be noted how the coefficients of Eq. 4 to Eq. 6 depend on the population means and variances of both classes, which causes different second-order surfaces for different *anomaly* and *background* pairs.

Finding the points in the moment space (plane in the two-dimensional case), for which the condition $Z = Z_0$ is satisfied, is equivalent to finding the projection of the cut between Z and plane $Z = Z_0$. This projection would be the curve that determines the decision boundary, whose exact shape depends on the coefficients in Eq. 4 to Eq. 6, resulting in ellipses or hyperbolas as shown in Fig. 1.
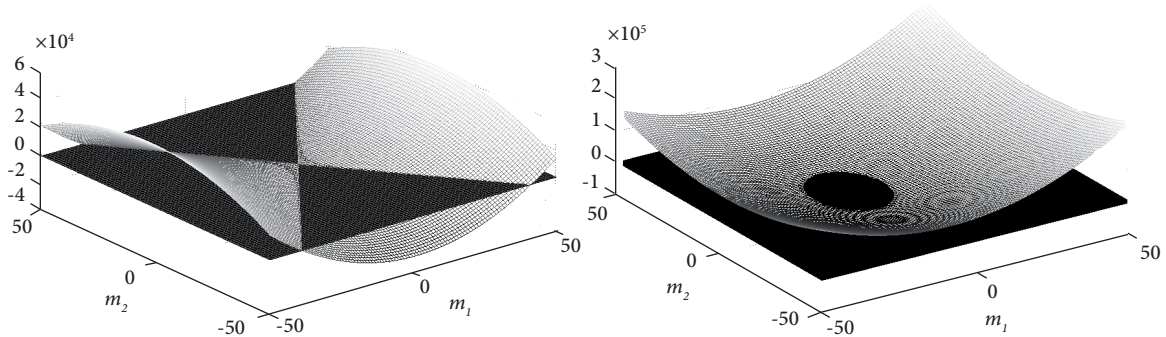
Figure 1. Intersection of the $Z=Z_o$ plane with the SDS to illustrate the different forms of the decision boundary. SDS = sufficient decision statistics.

From now on, we only consider the *background* and *anomaly* pairs whose SDS is an elliptical paraboloid, which causes the boundary to be an ellipse. The points in the moments plane for which $Z \geq Z_0$ are declared as *anomaly*, while those that comply with $Z < Z_0$ are declared as *background*. This reason can be more clearly illustrated by analyzing the one-dimensional case. Denoting the moment as m_s ($s = 1, 2$), the solutions of Eq. 3 can be expressed as:

$$m_{s,1,2} = A_s \pm \left(B_s + C_s Z_0\right)^{\frac{1}{2}} \tag{7}$$

where:

$$A_s = \frac{\left(\sigma_{A,s}^P\right)^2 m_{B,s}^P - \left(\sigma_{B,s}^P\right)^2 m_{A,s}^P}{\left(\sigma_{A,s}^P\right)^2 - \left(\sigma_{B,s}^P\right)^2} \tag{8}$$

$$B_s = \frac{\left[\left(\sigma_{B,s}^P\right)^2 m_{A,s}^P - \left(\sigma_{A,s}^P\right)^2 m_{B,s}^P\right]^2}{\left[\left(\sigma_{A,s}^P\right)^2 - \left(\sigma_{B,s}^P\right)^2\right]^2} - \frac{\left(\sigma_{A,s}^P\right)^2 \left(\sigma_{B,s}^P\right)^2}{\left(\sigma_{A,s}^P\right)^2 - \left(\sigma_{B,s}^P\right)^2} \left[\frac{\left(m_{B,s}^P\right)^2}{\left(\sigma_{B,s}^P\right)^2} - \frac{\left(m_{A,s}^P\right)^2}{\left(\sigma_{A,s}^P\right)^2}\right] \tag{9}$$

$$C_s = 2 \frac{\left(\sigma^P_{A,s}\right)^2 \left(\sigma^P_{B,s}\right)^2}{\left(\sigma^P_{A,s}\right)^2 - \left(\sigma^P_{B,s}\right)^2} \tag{10}$$

Figure 2 shows that the random variable Z will be a monotonically decreasing function of m_s in one case and a monotonically increasing function in the other, which means that for a threshold Z_0 corresponding to Λ_0, two thresholds m_{s01} and m_{s02} will be taken fulfilling that:

$$\Lambda(m_s) \geq \Lambda_0 \Leftrightarrow Z \geq Z_0 \Leftrightarrow (m_s \leq m_{s01}) \cup (m_s \geq m_{s02}) \tag{11}$$

Therefore, the moments can also be used directly as SDS.
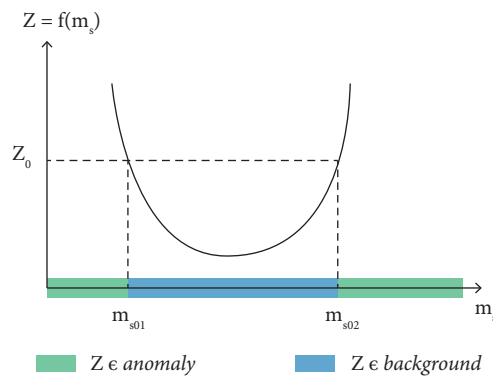
Figure 2. Relationship between the threshold of SDS Z_0 and the boundary in moment space (straight line in the one-dimensional case). SDS = sufficient decision statistics.

BOUNDARY SHAPE

As mentioned in the previous section, the boundary shape varies depending on the values of SDS coefficients. Although in this work only the case of the ellipse is considered, in the following discussion a methodology is established that allows to determine the general boundary shape for the two-dimensional case.

From the calculus theory, it is known that the general second order equation for two independent variables can be expressed as (Korn and Korn 1968):

$$ax^2 + cy^2 + 2dx + 2ey + 2bxy + f = 0 \tag{12}$$

where: x and y are the independent variables and the coefficients a, b, c, d, e and f determine the curve of the xy plane containing the points that satisfy the equation.

To know directly the shape of this curve from the coefficients, the invariants (Korn and Korn 1968) are calculated, which identify them univocally and are given by:
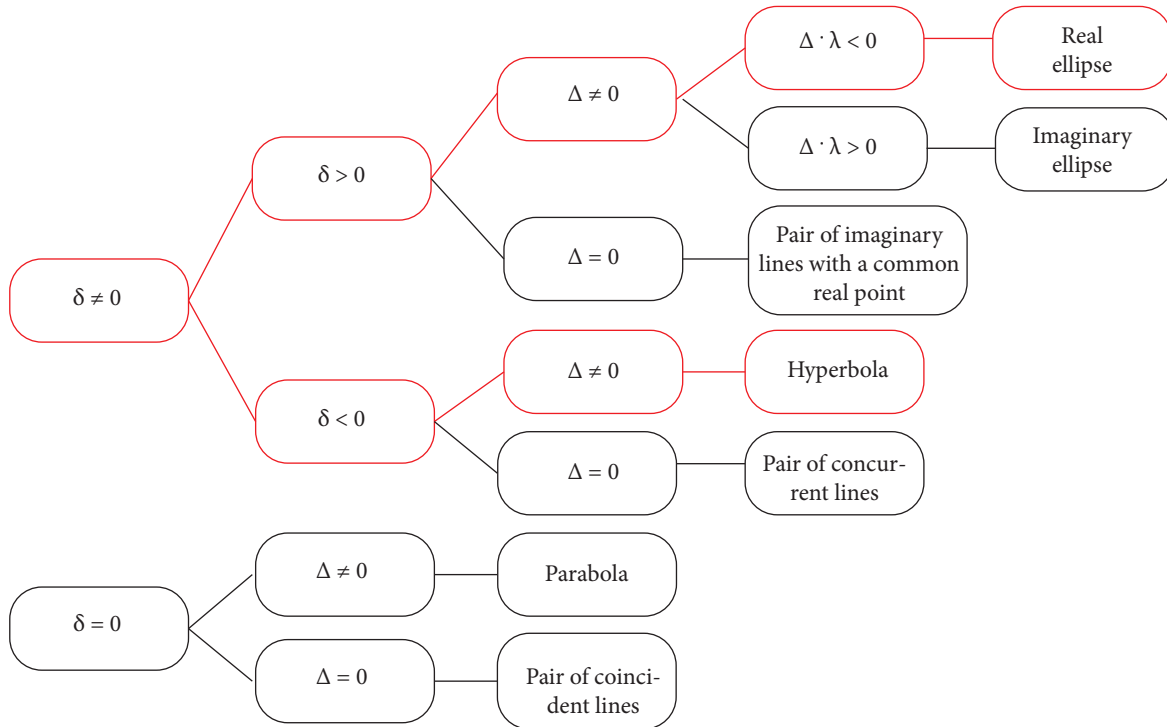
$$\Delta = \begin{vmatrix} a & b & d \\ b & c & e \\ d & e & f \end{vmatrix} \tag{13}$$

$$\delta = \begin{vmatrix} a & b \\ b & c \end{vmatrix} \tag{14}$$

$$\lambda = a + c \tag{15}$$

where: the $|.|$ operator denotes the determinant.

With the invariants, the conditions shown in Fig. 3 are verified to establish the curve type.

Figure 3. Curve types obtained according to the invariant's values.

Applying the previous concepts to the SDS case, Eq. 3 equals to Z_0 and the following invariants are obtained:

$$\Delta = \begin{vmatrix} a_1 & 0 & b_1/2 \\ 0 & a_2 & b_2/2 \\ b_1/2 & b_2/2 & c_1 + c_2 - Z_0 \end{vmatrix} = a_1 a_2 \left(c_1 + c_2 - Z_0 \right) - a_1 \left(\frac{b_2}{2} \right)^2 - a_2 \left(\frac{b_1}{2} \right)^2 \tag{16}$$

$$\delta = \begin{vmatrix} a_1 & 0 \\ 0 & a_2 \end{vmatrix} = a_1 a_2 \tag{17}$$

$$\lambda = a_1 + a_2 \tag{18}$$

As mentioned before, in this work only the red branches of Fig. 3 are of concern, since from the analysis of Eq. 4 and Eq. 17,

the remaining conditions are not probable or not practicable. For example, $\delta = 0$ requires that for any moment the population variance is the same for both classes, which is very unlikely. A similar reasoning stands for $\Delta = 0$.

According to Eq. 4 and Eq. 17, the elliptical boundary is obtained when the population variance for the *background* moments is less than that for the *anomaly* class. As will be seen by the simulations' results, this condition is common in the detection of a radiofrequency pulse in the presence of white Gaussian noise (Skolnik 2001; DiFranco and Rubin 2004; Richards *et al.* 2010), where the video signal under noise (*background*) has a Rayleigh distribution, while under target-plus-noise (*anomaly*) has a Rician distribution. When any moment of the *background* has a variance smaller than the *anomaly*, the corresponding coefficient of Eq. 4 will be negative, so the boundary could be a hyperbola and this case will be studied in a future work.

APPLICATION OF THE NEYMAN-PEARSON CRITERION

By setting a value for the false alarm probability P_{FA} and computing the R region of the moment space for which the Eq. 19 is satisfied, it is guaranteed that the P_D is maximum (Kay 1998; VanTrees *et al.* 2013).

$$1 - P_{FA} = \iint_R p_B\left(m_1\right) p_B\left(m_2\right) dm_1 dm_2 \tag{19}$$

Although Eq. 19 is valid for any boundary shape, here the R region is taken as the ellipse containing the *background* patterns, so the following procedures are only valid for this case. The ellipse will be formed by all the points in the moment plane satisfying the condition $Z=Z_0$ and its final size will depend on the P_{FA} since this regulates the Z_0 threshold. Therefore, we can determine the equation of the ellipse that conforms the boundary in Cartesian coordinates as:

$$\frac{\left(m_1 - \overset{o}{m}_1\right)^2}{l_1^2} + \frac{\left(m_2 - \overset{o}{m}_2\right)^2}{l_2^2} = 1 \tag{20}$$

where: $\overset{o}{m}_1$ and $\overset{o}{m}_2$ are the centroids, while l_1 and l_2 are the lengths of the semi-axes.

Making Eq. 3 equal to Z_0 and after several algebraic manipulations (Guillén 2013), we arrive at Eq. 21 and Eq. 22, which constitute the formulas to calculate the ellipse centroid and semi-axes, allowing us to know the boundary location and precise size.

$$\overset{o}{m}_s = -\frac{b_s}{2a_s} \qquad s = 1,\ 2 \tag{21}$$

$$l_s = \left(\frac{Z_0 - c_1 - c_2 + b_1^2/4a_1 + b_2^2/4a_2}{a_s}\right)^{\frac{1}{2}} = \left(\frac{Z_0'}{a_s}\right)^{\frac{1}{2}} \qquad s = 1,\ 2 \tag{22}$$

To simplify the computation of Eq. 19, the R region is taken as the rectangle in which the ellipse is inscribed, so that the calculated integral is:

$$1 - P_{FA} = \int_{\overset{o}{m}_1 - l_1}^{\overset{o}{m}_1 + l_1} p_B\left(m_1\right) dm_1 \int_{\overset{o}{m}_2 - l_2}^{\overset{o}{m}_2 + l_2} p_B\left(m_2\right) dm_2 \tag{23}$$

There is a loss in detection with this procedure, since the size of the integration zone is greater than the ellipse taken as boundary. This issue will be addressed in a future work.

The link between the threshold of SDS and the decision boundary in the moment space is clear from Eq. 22 and Eq. 23, since the final size of the ellipse will depend on the Z_0 value through Eq. 22, which, in turn, depends on the P_{FA} according to Eq. 23. The proposed algorithm for calculating the boundary would have the following steps:

1. Calculate the moments m_1 and m_2 for both classes, their population means and variances, as well as the SDS coefficients through Eq. 4 to Eq. 6.
2. Calculate the invariants and determine the boundary shape (ellipse in this work).
3. Choose a value of Z_0 and obtain the projection in the moment's plane that will be used to numerically evaluate the integral of Eq. 23.
4. Depending on whether the integral calculated in step 3 is greater or less than the required P_{FA}, the value of Z_0 is decreased or increased with a descendent-step algorithm (see the explanation bellow), and step 3 is repeated to re-calculate the integral over the new projection.
5. Repeat steps 3 and 4 until the Z_0 value guarantees the P_{FA}.

The algorithm to compute Z_0 is summarized in Fig. 4. The initial value for Z_0 is set to the minimum of the SDS and it is seen how the descendent-step algorithm works, through both control indicators (*flag*1 and *flag*2). In order to establish the Z_0 that ensures P_{FA}, the equality in Eq. 23 is verified with an error of four decimal digits, which could be modified as convenient. The variation of the step α proposed by this algorithm guarantees that Z_0 converges to the correct value. It is clarified that the double integral of Eq. 23 is denoted as I and is evaluated by the trapezoids method (Korn and Korn 1968).
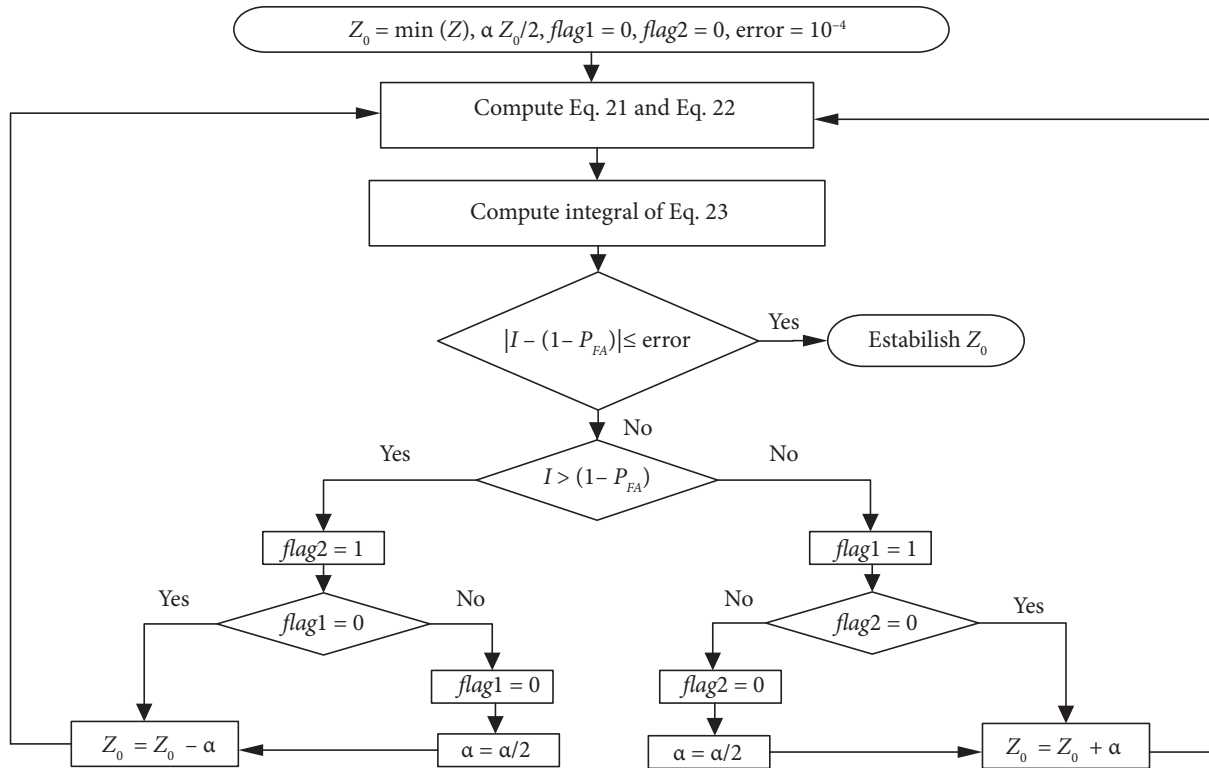
Figure 4. Flowchart of the algorithm to compute Z_0.

SIMULATIONS' RESULTS

To show the possibilities of the proposed methodology it is simulated by MATLAB (MathWorks 2015) an *anomaly-background* pair with the characteristics detailed next. The *background* is considered as the receiver internal noise, which is white, Gaussian, with zero mean, and total variance σ. Therefore, the amplitude x of the video signal for this class will be characterized by a Rayleigh PDF (Skolnik 2001) given by:

$$p_N(x) = \frac{x}{\sigma^2} \exp\left(-\frac{x^2}{2\sigma^2}\right) \tag{24}$$

On the other hand, the *anomaly* consists in the received radiofrequency pulses, so the amplitude x of the video stage under signal-plus-noise condition follows a Rice PDF (Skolnik 2001):

$$p_{S+N}(x) = I_0\left(\frac{xA}{\sigma^2}\right)\frac{x}{\sigma^2}\exp\left(-\frac{x^2 + A^2}{2\sigma^2}\right) \tag{25}$$

where: A is the maximum amplitude of the received pulse that will be detected and $I_0(\cdot)$ is the modified Bessel function of first kind and zero order.

This model corresponds with a non-fluctuating target, sometimes referred as Swerling 0 or Swerling V (Skolnik 2001; DiFranco and Rubin 2004; Richards *et al.* 2010).

To exemplify the boundary computation for one resolution cell, it is analyzed the behavior under both hypotheses of the video signal, which will be named hereafter as cellular emission. The selected moments are the mean and mean square (first and second order moments), both constituting a measure of the target radar cross-section and computed from 500 samples of the signal. Figure 5 shows the cellular emission behavior under both hypotheses, taking $\sigma = 1$ and $A = 0,4$ in Eq. 24 and Eq. 25. In the left it is observed one of the 1000 realizations of the process corresponding to the cellular emission, while in the right are the histograms of all samples. From the two graphs, it is verified the high similarity of the video signal under both hypotheses, what hinders the correct decision making.

On the other hand, the left part of Fig. 6 shows the 1000 patterns of the cellular emission (one for each realization) and the computed boundary for $P_{FA} = 10^{-6}$ by the procedure of the previous section. The right part shows the Gaussian joint PDF of the moments. From both graphs, it is appreciated how the analysis in the moments space could be used to increase the detection possibilities (Guillén 2013; Guillén and Chávez 2016; Chávez and Guillén 2018).
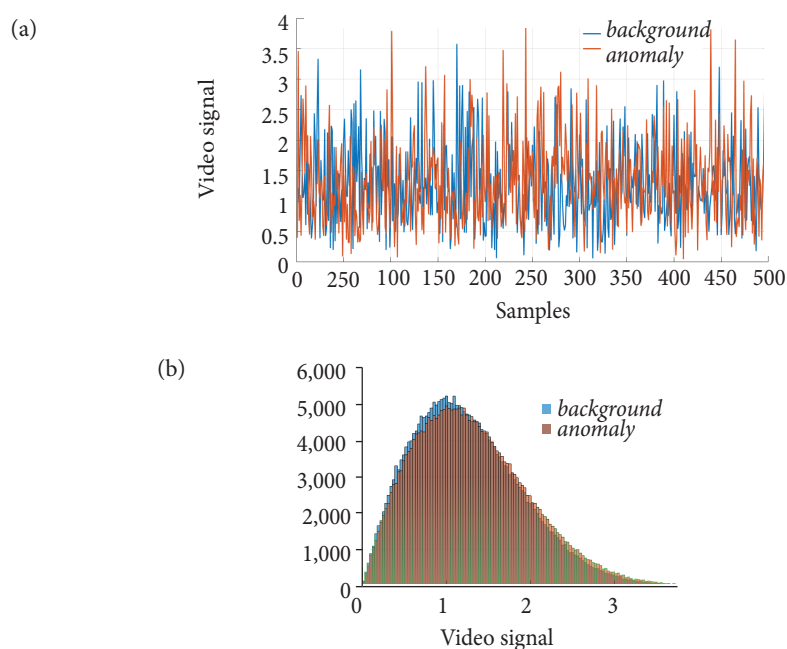
Figure 5. One realization of the cellular emission (a) and histogram (b) of the samples under both hypotheses: the *background* has a Rayleigh density with $\sigma = 1$ and the *anomaly* is Rician with $A = 0,4$ and $\sigma = 1$.
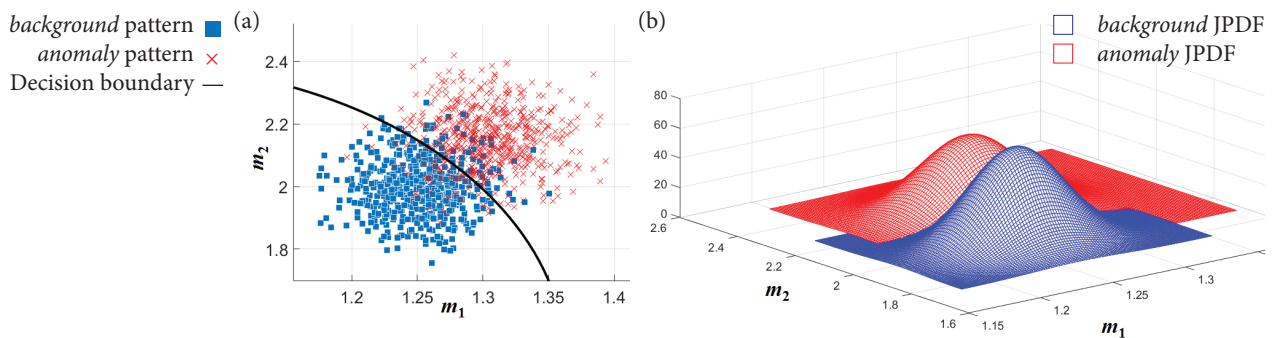
Figure 6. Decision boundary (a) for σ = 1, A = 0,4, and joint probability density functions (JPDF) (b) for both classes.

CONCLUSIONS

In the particular case of statistical independent moments, the SDS results in second-order hypersurfaces. The proposed algorithm allows us to calculate the ellipse boundary that guarantees the P_{FA} by applying the Neyman-Pearson criterion. Besides, the influence of SDS coefficients on the boundary shape will determine the characteristics and complexity of the algorithm.

Although the proposed methodology to determine the boundary shape is general, the algorithm to compute its size is a topic that should be thoroughly discussed in a future work, since the boundary can alternate typically between ellipse and hyperbola. This happens because the moments are random variables, and therefore the relationship between mean and population variance changes depending on the *background* and *anomaly* to be detected, especially in environments where there is great statistical similarity between both classes.

The multidimensional characteristic of detection by DRACEC allows envisaging important applications of this technique, especially in cases in which the dispersing properties of targets are similar to those of the environment that surrounds them. It is possible to ensure the above because, in general, the more statistical knowledge we have of the phenomena to be classified, which would be equivalent to using a great number of relevant features, the better the characterization of these, and therefore their classification.

AUTHOR'S CONTRIBUTION

Conceptualization, Chávez N; Methodology, Guillén C; Investigation, Guillén C; Writing – Original Draft, Guillén C; Writing – Review & Editing, Guillén C and Chávez N; Supervision, Chávez N.

FUNDERS

REFERENCES

Bishop CM (2006). Pattern Recognition and Machine Learning. Singapore: Springer.

Chávez N (2002) Detección y Alcance de Radar: La Alerta Temprana de Blancos en Fondos Enmascarantes y una Solución al Problema (PhD dissertation). La Habana: Instituto Técnico Militar "José Martí".

Chávez N, González AL (2008). Radar Recognition through Statistical Classification of Cellular Emission in the Moment Space. In: Ruiz-

Shulcloper J, Kropatsch WG, editors. Progress in Pattern Recognition, Image Analysis and Applications. CIARP 2008, LNCS 5197. Berlin, Heidelberg: Springer-Verlag.

Chávez N, Guillén C (2018) Radar Detection in the Moments Space of the Scattered Signal Parameters. Digital Signal Processing 83:359-366. https://doi.org/10.1016/j.dsp.2018.08.013

DiFranco JV, Rubin WL (2004) Radar Detection. Raleigh, NC: SciTech Publishing Inc.

Guillén C (2013) Determinación de la Frontera de Decisión y Evaluación de la Calidad de la Detección en el método DRACEC para dos momentos de la amplitud (BSc dissertation). La Habana: Instituto Superior Politécnico José Antonio Echeverría.

Guillén C, Chávez N (2016) Detección por Radar en el Espacio de los Momentos: Análisis de un Caso Particular. Paper presented at: VII Simposio Internacional de Telecomunicaciones, Informática 2016; La Habana, Cuba.

Kay SM (1998) Fundamentals of Statistical Signal Processing Volume II: Detection Theory. New Jersey: Prentice Hall.

Korn GA, Korn TM (1968) Mathematical Handbook for Scientists and Engineers. New York: McGraw-Hill Book Company.

Koroliuk VS (1981) Manual de la Teoría de Probabilidades y Estadística Matemática. Moscow: Editorial Mir.

MathWorks (2015). Matlab Help. ver R2015a.

Richards MA, Holm WA, Scheer JA (2010). Principles of Modern Radar Vol. I: Basic Principles. Raleigh, NC: SciTech Publishing.

Skolnik MI (2001). Introduction to Radar Systems. New York: McGraw-Hill.

VanTrees HL, Bell KL, Tian Z (2013). Detection, Estimation, and Modulation Theory Part I: Detection, Estimation, and Filtering Theory. Hoboken, NJ: John Wiley & Sons, Inc.

Webb A (2002) Statistical Pattern Recognition. Malvem, UK: John Wiley & Sons.